# Study of $J/\psi$ and $\psi(3686)$ decay to $\Lambda\bar{\Lambda}$ and $\Sigma^0\bar{\Sigma}^0$ final states

M. Ablikim,[1] M. N. Achasov,[9,e] S. Ahmed,[14] M. Albrecht,[4] A. Amoroso,[53a,53c] F. F. An,[1] Q. An,[50,a] J. Z. Bai,[1] Y. Bai,[39] O. Bakina,[24] R. Baldini Ferroli,[20a] Y. Ban,[32] D. W. Bennett,[19] J. V. Bennett,[5] N. Berger,[23] M. Bertani,[20a] D. Bettoni,[21a] J. M. Bian,[47] F. Bianchi,[53a,53c] E. Boger,[24,c] I. Boyko,[24] R. A. Briere,[5] H. Cai,[55] X. Cai,[1,a] O. Cakir,[43a] A. Calcaterra,[20a] G. F. Cao,[1] S. A. Cetin,[43b] J. Chai,[53c] J. F. Chang,[1,a] G. Chelkov,[24,c,d] G. Chen,[1] H. S. Chen,[1] J. C. Chen,[1] M. L. Chen,[1,a] S. J. Chen,[30] X. R. Chen,[27] Y. B. Chen,[1,a] X. K. Chu,[32] G. Cibinetto,[21a] H. L. Dai,[1,a] J. P. Dai,[35,j] A. Dbeyssi,[14] D. Dedovich,[24] Z. Y. Deng,[1] A. Denig,[23] I. Denysenko,[24] M. Destefanis,[53a,53c] F. De Mori,[53a,53c] Y. Ding,[28] C. Dong,[31] J. Dong,[1,a] L. Y. Dong,[1] M. Y. Dong,[1,a] O. Dorjkhaidav,[22] Z. L. Dou,[30] S. X. Du,[57] P. F. Duan,[1] J. Fang,[1,a] S. S. Fang,[1] X. Fang,[50,a] Y. Fang,[1] R. Farinelli,[21a,21b] L. Fava,[53b,53c] S. Fegan,[23] F. Feldbauer,[23] G. Felici,[20a] C. Q. Feng,[50,a] E. Fioravanti,[21a] M. Fritsch,[14,23] C. D. Fu,[1] Q. Gao,[1] X. L. Gao,[50,a] Y. Gao,[42] Y. G. Gao,[6] Z. Gao,[50,a] I. Garzia,[21a] K. Goetzen,[10] L. Gong,[31] W. X. Gong,[1,a] W. Gradl,[23] M. Greco,[53a,53c] M. H. Gu,[1,a] S. Gu,[15] Y. T. Gu,[12] A. Q. Guo,[1] L. B. Guo,[29] R. P. Guo,[1] Y. P. Guo,[23] Z. Haddadi,[26] S. Han,[55] X. Q. Hao,[15] F. A. Harris,[45] K. L. He,[1] X. Q. He,[49] F. H. Heinsius,[4] T. Held,[4] Y. K. Heng,[1,a] T. Holtmann,[4] Z. L. Hou,[1] C. Hu,[29] H. M. Hu,[1] T. Hu,[1,a] Y. Hu,[1] G. S. Huang,[50,a] J. S. Huang,[15] X. T. Huang,[34] X. Z. Huang,[30] Z. L. Huang,[28] T. Hussain,[52] W. Ikegami Andersson,[54] Q. Ji,[1] Q. P. Ji,[15] X. B. Ji,[1] X. L. Ji,[1,a] X. S. Jiang,[1,a] X. Y. Jiang,[31] J. B. Jiao,[34] Z. Jiao,[17] D. P. Jin,[1,a] S. Jin,[1] Y. Jin,[46] T. Johansson,[54] A. Julin,[47] N. Kalantar-Nayestanaki,[26] X. L. Kang,[1] X. S. Kang,[31] M. Kavatsyuk,[26] B. C. Ke,[5] T. Khan,[50,a] A. Khoukaz,[48] P. Kiese,[23] R. Kliemt,[10] L. Koch,[25] O. B. Kolcu,[43b,h] B. Kopf,[4] M. Kornicer,[45] M. Kuemmel,[4] M. Kuhlmann,[4] A. Kupsc,[54] W. Kühn,[25] J. S. Lange,[25] M. Lara,[19] P. Larin,[14] L. Lavezzi,[53c,1] H. Leithoff,[23] C. Leng,[53c] C. Li,[54] Cheng Li,[50,a] D. M. Li,[57] F. Li,[1,a] F. Y. Li,[32] G. Li,[1] H. B. Li,[1] H. J. Li,[1] J. C. Li,[1] Jin Li,[33] K. Li,[34] K. Li,[13] K. J. Li,[41] Lei Li,[3] P. L. Li,[50,a] P. R. Li,[7,44] Q. Y. Li,[34] T. Li,[34] W. D. Li,[1] W. G. Li,[1] X. L. Li,[34] X. N. Li,[1,a] X. Q. Li,[31] Z. B. Li,[41] H. Liang,[50,a] Y. F. Liang,[37] Y. T. Liang,[25] G. R. Liao,[11] D. X. Lin,[14] B. Liu,[35,j] B. J. Liu,[1] C. X. Liu,[1] D. Liu,[50,a] F. H. Liu,[36] Fang Liu,[1] Feng Liu,[6] H. B. Liu,[12] H. H. Liu,[16] H. H. Liu,[1] H. M. Liu,[1] J. B. Liu,[50,a] J. P. Liu,[55] J. Y. Liu,[1] K. Liu,[42] K. Y. Liu,[28] Ke Liu,[6] L. D. Liu,[32] P. L. Liu,[1,a] Q. Liu,[44] S. B. Liu,[50,a] X. Liu,[27] Y. B. Liu,[31] Y. Y. Liu,[31] Z. A. Liu,[1,a] Zhiqing Liu,[23] Y. F. Long,[32] X. C. Lou,[1,a,g] H. J. Lu,[17] J. G. Lu,[1,a] Y. Lu,[1] Y. P. Lu,[1,a] C. L. Luo,[29] M. X. Luo,[56] X. L. Luo,[1,a] X. R. Lyu,[44] F. C. Ma,[28] H. L. Ma,[1] L. L. Ma,[34] M. M. Ma,[1] Q. M. Ma,[1] T. Ma,[1] X. N. Ma,[31] X. Y. Ma,[1,a] Y. M. Ma,[34] F. E. Maas,[14] M. Maggiora,[53a,53c] Q. A. Malik,[52] Y. J. Mao,[32] Z. P. Mao,[1] S. Marcello,[53a,53c] Z. X. Meng,[46] J. G. Messchendorp,[26] G. Mezzadri,[21b] J. Min,[1,a] T. J. Min,[1] R. E. Mitchell,[19] X. H. Mo,[1,a] Y. J. Mo,[6] C. Morales Morales,[14] G. Morello,[20a] N. Yu. Muchnoi,[9,e] H. Muramatsu,[47] P. Musiol,[4] A. Mustafa,[4] Y. Nefedov,[24] F. Nerling,[10] I. B. Nikolaev,[9,e] Z. Ning,[1,a] S. Nisar,[8] S. L. Niu,[1,a] X. Y. Niu,[1] S. L. Olsen,[33] Q. Ouyang,[1,a] S. Pacetti,[20b] Y. Pan,[50,a] P. Patteri,[20a] M. Pelizaeus,[4] J. Pellegrino,[53a,53c] H. P. Peng,[50,a] K. Peters,[10,i] J. Pettersson,[54] J. L. Ping,[29] R. G. Ping,[1] R. Poling,[47] V. Prasad,[40,50] H. R. Qi,[2] M. Qi,[30] S. Qian,[1,a] C. F. Qiao,[44] J. J. Qin,[44] N. Qin,[55] X. S. Qin,[1] Z. H. Qin,[1,a] J. F. Qiu,[1] K. H. Rashid,[52,k] C. F. Redmer,[23] M. Richter,[4] M. Ripka,[23] M. Rolo,[53c] G. Rong,[1] Ch. Rosner,[14] X. D. Ruan,[12] A. Sarantsev,[24,f] M. Savrié,[21b] C. Schnier,[4] K. Schoenning,[54] W. Shan,[32] M. Shao,[50,a] C. P. Shen,[2] P. X. Shen,[31] X. Y. Shen,[1] H. Y. Sheng,[1] J. J. Song,[34] X. Y. Song,[1] S. Sosio,[53a,53c] C. Sowa,[4] S. Spataro,[53a,53c] G. X. Sun,[1] J. F. Sun,[15] L. Sun,[55] S. S. Sun,[1] X. H. Sun,[1] Y. J. Sun,[50,a] Y. K. Sun,[50,a] Y. Z. Sun,[1] Z. J. Sun,[1,a] Z. T. Sun,[19] C. J. Tang,[37] G. Y. Tang,[1] X. Tang,[1] I. Tapan,[43c] M. Tiemens,[26] B. T. Tsednee,[22] I. Uman,[43d] G. S. Varner,[45] B. Wang,[1] B. L. Wang,[44] D. Wang,[32] D. Y. Wang,[32] Dan Wang,[44] K. Wang,[1,a] L. L. Wang,[1] L. S. Wang,[1] M. Wang,[34] P. Wang,[1] P. L. Wang,[1] W. P. Wang,[50,a] X. F. Wang,[42] Y. D. Wang,[14] Y. F. Wang,[1,a] Y. Q. Wang,[23] Z. Wang,[1,a] Z. G. Wang,[1,a] Z. H. Wang,[50,a] Z. Y. Wang,[1] Z. Y. Wang,[1] T. Weber,[23] D. H. Wei,[11] P. Weidenkaff,[23] S. P. Wen,[1] U. Wiedner,[4] M. Wolke,[54] L. H. Wu,[1] L. J. Wu,[1] Z. Wu,[1,a] L. Xia,[50,a] Y. Xia,[18] D. Xiao,[1] H. Xiao,[51] Y. J. Xiao,[1] Z. J. Xiao,[29] Y. G. Xie,[1,a] Y. H. Xie,[6] X. A. Xiong,[1] Q. L. Xiu,[1,a] G. F. Xu,[1] J. J. Xu,[1] L. Xu,[1] Q. J. Xu,[13] Q. N. Xu,[44] X. P. Xu,[38] L. Yan,[53a,53c] W. B. Yan,[50,a] W. C. Yan,[50,a] Y. H. Yan,[18] H. J. Yang,[35,j] H. X. Yang,[1] L. Yang,[55] Y. H. Yang,[30] Y. X. Yang,[11] M. Ye,[1,a] M. H. Ye,[7] J. H. Yin,[1] Z. Y. You,[41] B. X. Yu,[1,a] C. X. Yu,[31] J. S. Yu,[27] C. Z. Yuan,[1] Y. Yuan,[1] A. Yuncu,[43b,b] A. A. Zafar,[52] Y. Zeng,[18] Z. Zeng,[50,a] B. X. Zhang,[1] B. Y. Zhang,[1,a] C. C. Zhang,[1] D. H. Zhang,[1] H. H. Zhang,[41] H. Y. Zhang,[1,a] J. Zhang,[1] J. L. Zhang,[1] J. Q. Zhang,[1] J. W. Zhang,[1,a] J. Y. Zhang,[1] J. Z. Zhang,[1] K. Zhang,[1] L. Zhang,[42] S. Q. Zhang,[31] X. Y. Zhang,[34] Y. Zhang,[1] Y. Zhang,[1] Y. H. Zhang,[1,a] Y. T. Zhang,[50,a] Yu Zhang,[44] Z. H. Zhang,[6] Z. P. Zhang,[50] Z. Y. Zhang,[55] G. Zhao,[1] J. W. Zhao,[1,a] J. Y. Zhao,[1] J. Z. Zhao,[1,a] Lei Zhao,[50,a] Ling Zhao,[1] M. G. Zhao,[31] Q. Zhao,[1] S. J. Zhao,[57] T. C. Zhao,[1] Y. B. Zhao,[1,a] Z. G. Zhao,[50,a] A. Zhemchugov,[24,c] B. Zheng,[14,51] J. P. Zheng,[1,a] W. J. Zheng,[34] Y. H. Zheng,[44] B. Zhong,[29] L. Zhou,[1,a] X. Zhou,[55] X. K. Zhou,[50,a] X. R. Zhou,[50,a] X. Y. Zhou,[1] Y. X. Zhou,[12,a] J. Zhu,[41] K. Zhu,[1] K. J. Zhu,[1,a] S. Zhu,[1] S. H. Zhu,[49] X. L. Zhu,[42] Y. C. Zhu,[50,a] Y. S. Zhu,[1] Z. A. Zhu,[1] J. Zhuang,[1,a] L. Zotti,[53a,53c] B. S. Zou,[1] and J. H. Zou[1]

(BESIII Collaboration)

[1]*Institute of High Energy Physics, Beijing 100049, People's Republic of China*
[2]*Beihang University, Beijing 100191, People's Republic of China*

 

[3]*Beijing Institute of Petrochemical Technology, Beijing 102617, People's Republic of China*
[4]*Bochum Ruhr-University, D-44780 Bochum, Germany*
[5]*Carnegie Mellon University, Pittsburgh, Pennsylvania 15213, USA*
[6]*Central China Normal University, Wuhan 430079, People's Republic of China*
[7]*China Center of Advanced Science and Technology, Beijing 100190, People's Republic of China*
[8]*COMSATS Institute of Information Technology, 54000 Lahore, Pakistan*
[9]*G.I. Budker Institute of Nuclear Physics SB RAS (BINP), Novosibirsk 630090, Russia*
[10]*GSI Helmholtzcentre for Heavy Ion Research GmbH, D-64291 Darmstadt, Germany*
[11]*Guangxi Normal University, Guilin 541004, People's Republic of China*
[12]*Guangxi University, Nanning 530004, People's Republic of China*
[13]*Hangzhou Normal University, Hangzhou 310036, People's Republic of China*
[14]*Helmholtz Institute Mainz, D-55099 Mainz, Germany*
[15]*Henan Normal University, Xinxiang 453007, People's Republic of China*
[16]*Henan University of Science and Technology, Luoyang 471003, People's Republic of China*
[17]*Huangshan College, Huangshan 245000, People's Republic of China*
[18]*Hunan University, Changsha 410082, People's Republic of China*
[19]*Indiana University, Bloomington, Indiana 47405, USA*
[20a]*INFN Laboratori Nazionali di Frascati, I-00044 Frascati, Italy*
[20b]*INFN and University of Perugia, I-06100 Perugia, Italy*
[21a]*INFN Sezione di Ferrara, I-44122 Ferrara, Italy*
[21b]*University of Ferrara, I-44122 Ferrara, Italy*
[22]*Institute of Physics and Technology, Ulaanbaatar 13330, Mongolia*
[23]*Johannes Gutenberg University of Mainz, D-55099 Mainz, Germany*
[24]*Joint Institute for Nuclear Research, 141980 Dubna, Moscow region, Russia*
[25]*Justus-Liebig-Universitaet Giessen, II. Physikalisches Institut, D-35392 Giessen, Germany*
[26]*KVI-CART, University of Groningen, NL-9747 AA Groningen, Netherlands*
[27]*Lanzhou University, Lanzhou 730000, People's Republic of China*
[28]*Liaoning University, Shenyang 110036, People's Republic of China*
[29]*Nanjing Normal University, Nanjing 210023, People's Republic of China*
[30]*Nanjing University, Nanjing 210093, People's Republic of China*
[31]*Nankai University, Tianjin 300071, People's Republic of China*
[32]*Peking University, Beijing 100871, People's Republic of China*
[33]*Seoul National University, Seoul 151-747, Korea*
[34]*Shandong University, Jinan 250100, People's Republic of China*
[35]*Shanghai Jiao Tong University, Shanghai 200240, People's Republic of China*
[36]*Shanxi University, Taiyuan 030006, People's Republic of China*
[37]*Sichuan University, Chengdu 610064, People's Republic of China*
[38]*Soochow University, Suzhou 215006, People's Republic of China*
[39]*Southeast University, Nanjing 211100, People's Republic of China*
[40]*State Key Laboratory of Particle Detection and Electronics, Beijing 100049, Hefei 230026, People's Republic of China*
[41]*Sun Yat-Sen University, Guangzhou 510275, People's Republic of China*
[42]*Tsinghua University, Beijing 100084, People's Republic of China*
[43a]*Ankara University, 06100 Tandogan, Ankara, Turkey*
[43b]*Istanbul Bilgi University, 34060 Eyup, Istanbul, Turkey*
[43c]*Uludag University, 16059 Bursa, Turkey*
[43d]*Near East University, Nicosia, North Cyprus, Mersin 10, Turkey*
[44]*University of Chinese Academy of Sciences, Beijing 100049, People's Republic of China*
[45]*University of Hawaii, Honolulu, Hawaii 96822, USA*
[46]*University of Jinan, Jinan 250022, People's Republic of China*
[47]*University of Minnesota, Minneapolis, Minnesota 55455, USA*
[48]*University of Muenster, 48149 Muenster, Germany*
[49]*University of Science and Technology Liaoning, Anshan 114051, People's Republic of China*
[50]*University of Science and Technology of China, Hefei 230026, People's Republic of China*
[51]*University of South China, Hengyang 421001, People's Republic of China*
[52]*University of the Punjab, Lahore 54590, Pakistan*
[53a]*University of Turin, I-10125 Turin, Italy*
[53b]*University of Eastern Piedmont, I-15121 Alessandria, Italy*
[53c]*INFN, I-10125 Turin, Italy*
[54]*Uppsala University, Box 516, SE-75120 Uppsala, Sweden*

[55]Wuhan University, Wuhan 430072, People's Republic of China
[56]Zhejiang University, Hangzhou 310027, People's Republic of China
[57]Zhengzhou University, Zhengzhou 450001, People's Republic of China
(Received 25 January 2017; published 15 March 2017)

Using $1310.6 \times 10^6$ $J/\psi$ and $447.9 \times 10^6$ $\psi(3686)$ events collected with the BESIII detector at the BEPCII $e^+e^-$ collider, the branching fractions and the angular distributions of $J/\psi$ and $\psi(3686)$ decays to $\Lambda\bar{\Lambda}$ and $\Sigma^0\bar{\Sigma}^0$ final states are measured. The branching fractions are determined, with much improved precision, to be $19.43 \pm 0.03 \pm 0.33$, $11.64 \pm 0.04 \pm 0.23$, $3.97 \pm 0.02 \pm 0.12$ and $2.44 \pm 0.03 \pm 0.11$ for $J/\psi \to \Lambda\bar{\Lambda}$, $J/\psi \to \Sigma^0\bar{\Sigma}^0$, $\psi(3686) \to \Lambda\bar{\Lambda}$ and $\psi(3686) \to \Sigma^0\bar{\Sigma}^0$, respectively. The polar angular distributions of $\psi(3686)$ decays are measured for the first time, while those of $J/\psi$ decays are measured with much improved precision. In addition, the ratios of branching fractions $\frac{\mathcal{B}(\psi(3686)\to\Lambda\bar{\Lambda})}{\mathcal{B}(J/\psi\to\Lambda\bar{\Lambda})}$ and $\frac{\mathcal{B}(\psi(3686)\to\Sigma^0\bar{\Sigma}^0)}{\mathcal{B}(J/\psi\to\Sigma^0\bar{\Sigma}^0)}$ are determined to test the "12% rule."

DOI: 10.1103/PhysRevD.95.052003

## I. INTRODUCTION

Two-body baryonic decays of $\psi$ mesons [$\psi$ denotes both the $J/\psi$ and $\psi(3686)$ charmonium states throughout the text] take place through annihilation of the constituent $c\bar{c}$ quark pair into either a virtual photon or three gluons, and they provide a good laboratory for testing quantum chromodynamics (QCD) in the perturbative energy regime and studying the properties of baryons [1]. Perturbative QCD (pQCD) predicts that the ratio of branching fractions between the $J/\psi$ and $\psi(3686)$ decaying into a given hadronic final states follows the "12% rule" [2]

$$Q = \frac{\mathcal{B}_{\psi(3686)\to h}}{\mathcal{B}_{J/\psi\to h}} = \frac{\mathcal{B}_{\psi(3686)\to l^+l^-}}{\mathcal{B}_{J/\psi\to l^+l^-}} \approx (12.4 \pm 0.4)\%. \quad (1)$$

The violation of this rule was first observed in the decay of $\psi$ into the final state $\rho\pi$, which is well known as the "$\rho\pi$ puzzle" [3], and the rule has been subsequently further tested in a wide variety of experimental measurements. Reviews of the theoretical and experimental results [4] conclude that the current theoretical understanding, especially for the $\psi$ decays into baryon-antibaryon pair final states, is not mature. The branching fractions of $\psi$ decays into $B\bar{B}$ ($B\bar{B}$ refers to both $\Lambda\bar{\Lambda}$ and $\Sigma^0\bar{\Sigma}^0$ throughout the text) final states from different experiments [5–14] and the Particle Data Group (PDG) [15] averages are summarized in Table I. Obvious differences between the different experiments are observed, and the uncertainties are relatively large. Hence, higher precision measurements of the $\psi$ decays into $B\bar{B}$ pairs are desirable to help in understanding the dynamics of $\psi$ decay.

The angular distribution of the decays $e^+e^- \to \psi \to B\bar{B}$ can be expressed in the form [1]

$$\frac{dN}{d\cos\theta} \propto 1 + \alpha\cos^2\theta, \quad (2)$$

where $\theta$ is the angle between the outgoing baryon and the beam direction in the $e^+e^-$ center-of-mass (c.m.) system and $\alpha$ is a constant that is related to the decay properties. The equation is derived from the general helicity formalism [1], taking into account the gluon spin, the quark distribution amplitudes in $e^+e^- \to \psi \to B\bar{B}$ and hadron helicity conservation. The $\alpha$ values in the decays $J/\psi \to B\bar{B}$ have been calculated with pQCD to first order [16]. It is believed that the masses of the baryon and quark must be taken into consideration in the $\alpha$ calculation since a large violation of helicity conservation is observed in $\psi$ decays [16,17]. Table II summarizes the theoretical predictions and experimental $\alpha$ values for the decays $J/\psi \to B\bar{B}$. To date, the experimental $\alpha$ values for the decays $J/\psi \to B\bar{B}$ have poor precision [5,6,10], and the $\alpha$ values in the decay $\psi(3686) \to B\bar{B}$ have not yet been measured. It is worth noting that there is an indication that the $\alpha$ value in the decay $J/\psi \to \Sigma^0\bar{\Sigma}^0$ is negative in Ref. [10].

[a]Also at State Key Laboratory of Particle Detection and Electronics, Beijing 100049, Hefei 230026, People's Republic of China.
[b]Also at Bogazici University, 34342 Istanbul, Turkey.
[c]Also at Moscow Institute of Physics and Technology, Moscow 141700, Russia.
[d]Also at Functional Electronics Laboratory, Tomsk State University, Tomsk 634050, Russia.
[e]Also at Novosibirsk State University, Novosibirsk 630090, Russia.
[f]Also at NRC "Kurchatov Institute," PNPI, 188300 Gatchina, Russia.
[g]Also at University of Texas at Dallas, Richardson, Texas 75083, USA.
[h]Also at Istanbul Arel University, 34295 Istanbul, Turkey.
[i]Also at Goethe University Frankfurt, 60323 Frankfurt am Main, Germany.
[j]Also at Key Laboratory for Particle Physics, Astrophysics and Cosmology, Ministry of Education; Shanghai Key Laboratory for Particle Physics and Cosmology; and Institute of Nuclear and Particle Physics, Shanghai 200240, People's Republic of China.
[k]Government College Women University, Sialkot, 51310 Punjab, Pakistan.

TABLE I. Experimental measurements and PDG averages for the branching fractions of the decay $\psi \to B\bar{B}$ ($\times 10^{-4}$).

| | $J/\psi \to \Lambda\bar{\Lambda}$ | $\psi(3686) \to \Lambda\bar{\Lambda}$ | $J/\psi \to \Sigma^0\bar{\Sigma}^0$ | $\psi(3686) \to \Sigma^0\bar{\Sigma}^0$ |
|---|---|---|---|---|
| MARKII Collaboration [5] | $15.8 \pm 0.8 \pm 1.9$ | ... | $15.8 \pm 1.6 \pm 2.5$ | ... |
| DM2 Collaboration [6] | $13.8 \pm 0.5 \pm 2.0$ | ... | $10.6 \pm 0.4 \pm 2.3$ | ... |
| BES Collaboration [7,8] | $10.8 \pm 0.6 \pm 2.4$ | $1.8 \pm 0.2 \pm 0.3$ | ... | $1.2 \pm 0.4 \pm 0.4$ |
| CLEO Collaboration [9] | ... | $3.3 \pm 0.3 \pm 0.3$ | ... | $2.6 \pm 0.4 \pm 0.4$ |
| BESII Collaboration [10,11] | $20.3 \pm 0.3 \pm 1.5$ | $3.4 \pm 0.2 \pm 0.4$ | $13.3 \pm 0.4 \pm 1.1$ | $2.4 \pm 0.4 \pm 0.4$ |
| *BABAR* Collaboration [12] | $19.3 \pm 2.1 \pm 0.5$ | $6.4 \pm 1.8 \pm 0.1$ | $11.5 \pm 2.4 \pm 0.3$ | ... |
| Dobbs *et al.* [13] | ... | $3.8 \pm 0.1 \pm 0.3$ | ... | $2.3 \pm 0.2 \pm 0.2$ |
| PDG [15] | $16.1 \pm 1.5$ | $3.6 \pm 0.2$ | $12.9 \pm 0.9$ | $2.3 \pm 0.2$ |

TABLE II. Theoretical predictions and experimental measurements of $\alpha$ for $J/\psi \to B\bar{B}$.

| | $\alpha_{J/\psi\to\Lambda\bar{\Lambda}}$ | $\alpha_{J/\psi\to\Sigma^0\bar{\Sigma}^0}$ |
|---|---|---|
| Theory | 0.32 | 0.31 [16] |
| | 0.51 | 0.43 [17] |
| Experiment | $0.72 \pm 0.36$ | $0.70 \pm 1.10$ [5] |
| | $0.62 \pm 0.22$ | $0.22 \pm 0.31$ [6] |
| | $0.65 \pm 0.14$ | $-0.22 \pm 0.19$ [10] |

In this paper, we report precise measurements of the branching fractions and $\alpha$ values for the decays $\psi \to B\bar{B}$, based on the data samples of $(1310.6 \pm 7.0) \times 10^6$ $J/\psi$ [18] and $(447.9 \pm 2.9) \times 10^6$ $\psi(3686)$ [19,20] events collected with the BESIII detector at the BEPCII collider.

## II. BESIII DETECTOR AND DATA SET

The BESIII detector [21] at the double-ring Beijing Electron-Positron Collider (BEPCII) [22] is designed for studies of physics in the $\tau$-charm energy region [23]. The peak luminosity of BEPCII is $10^{33}$ cm$^{-2}$ s$^{-1}$ at a beam current of 0.93 A. The BESIII detector has a geometrical acceptance of 93% of $4\pi$ solid angle and consists of the following main components: (1) A small-celled, helium-based (40% $CO_2$ and 60% $C_3H_8$) main drift chamber with 43 layers, which has an average single-wire resolution of 135 $\mu$m, a momentum resolution for 1 GeV/c charged particles in a 1 T magnetic field of 0.5%,[1] and a specific energy loss ($dE/dx$) resolution of better than 6%. (2) An electromagnetic calorimeter (EMC), which consists of 6240 CsI (Tl) crystals arranged in a cylindrical shape (barrel) plus two end caps. For 1.0 GeV photons, the energy resolution is 2.5% (5%) in the barrel (end caps), and the position resolution is 6 mm (9 mm) for the barrel (end caps). (3) A time-of-flight (TOF) system, which is used for particle identification. It is composed of a barrel made of two layers, each consisting of 88 pieces of 5-cm-thick and 2.4-m-long plastic scintillators, as well as two end caps each with 96 fan-shaped 5-cm-thick plastic scintillators. The time resolution is 80 ps (110 ps) in the barrel (end caps), providing a $K/\pi$ separation of more than $2\sigma$ for momenta up to 1.0 GeV/c. (4) A muon chamber system, which is made of resistive plate chamber arranged in 9 layers (8 layers) in the barrel (end caps) with ~2 cm position resolution. It is incorporated into the return iron yoke of the superconducting magnet.

The optimization of the event selection and the estimations of the signal detection efficiency and background are determined using Monte Carlo (MC) simulations. The GEANT4-based [24] simulation software BOOST [25], which includes the geometric and material description of the BESIII detector, the detector response and digitization models, as well as the tracking of the detector running conditions and performance, is used to generate MC samples. The analysis is performed in the framework of the BESIII offline software system [26] which takes care of the detector calibration, event reconstruction and data storage.

Generic inclusive MC samples, which include $1225 \times 10^6$ $J/\psi$ and $460 \times 10^6$ $\psi(3686)$ events, are used to study the potential backgrounds. The $\psi$ are produced via $e^+e^- \to \psi$ processes by the generator KKMC [27], which includes the beam energy spread according to the measurement of BEPCII and the effect of initial state radiation. The known decay modes are generated with BesEvtGen [28] according to world average branching fraction values [15]; the remaining unknown decay modes are simulated using the LundCharm model [29]. To determine the detection efficiencies, large $\psi \to B\bar{B}$ signal MC samples are generated for each process, where the angular distributions of the baryons use $\alpha$ values obtained in this analysis. The $\Lambda$ and $\Sigma^0$ particles are simulated in the $\Lambda \to p\pi^-$ and $\Sigma^0 \to \gamma\Lambda$ decay modes.

## III. EVENT SELECTION

In this analysis, the four decay modes $\psi \to B\bar{B}$ are studied by fully reconstructing both $B$ and $\bar{B}$, where the $\Lambda(\bar{\Lambda})$ and $\Sigma^0(\bar{\Sigma}^0)$ candidates are reconstructed with the $p\pi^-(\bar{p}\pi^+)$ and $\gamma\Lambda(\gamma\bar{\Lambda})$ decay modes, respectively. Therefore, the decays $\psi \to \Lambda\bar{\Lambda}$ and $\psi \to \Sigma^0\bar{\Sigma}^0$ have the final states $p\bar{p}\pi^+\pi^-$ and $p\bar{p}\pi^+\pi^-\gamma\gamma$, respectively.

[1]For the $J/\psi$ data sample collected in 2012, the magnetic field was 0.9 T.

Events with at least four charged tracks with total charge zero are selected. Each charged track is required to have $|\cos\theta| < 0.93$, where $\theta$ is the polar angle of the track. Photons are reconstructed from isolated showers in the EMC which are at least 30 degrees away from the antiproton and 10 degrees from other charged tracks. The energy deposited in the nearby TOF counters is included to improve the photon reconstruction efficiency and energy resolution. Photon candidates are required to be within the barrel region ($|\cos\theta| < 0.8$) of the EMC with deposited energy of at least 25 MeV, or within the end cap regions ($0.86 < |\cos\theta| < 0.92$) with at least 50 MeV, where $\theta$ is the polar angle of the photon. In order to suppress electronic noise and energy deposits unrelated to the event, the timing information $t$ from the EMC for the photon candidate must be in coincidence with the collision event ($0 \le t \le 700$ ns). At least two photons are required in the analysis of $\psi \to \Sigma^0\bar{\Sigma}^0$ decays.

MC studies indicate that the proton and pion from $\Lambda$ decay are well separated kinematically since the proton carries most of the energy. A charged track with momentum $p > 0.5$ GeV/c is assumed to be a proton, while that with $p < 0.5$ GeV/c is assumed to be a pion. The $\Lambda$ ($\bar{\Lambda}$) candidate is reconstructed with any $p\pi^-$ ($\bar{p}\pi^+$) combination satisfying a secondary vertex fit [30] and having a decay length larger than 0.2 cm to suppress the non-$\Lambda$ (non-$\bar{\Lambda}$) decays. The decay length is the distance between its primary vertex and decay point to $p\pi^-$ ($\bar{p}\pi^+$), where the primary vertex is approximated by the interaction point averaged over many events. If more than one $\Lambda$ ($\bar{\Lambda}$) candidate is found, the one with the largest decay length is retained for further analysis.

In the study of $\psi \to \Sigma^0\bar{\Sigma}^0$ decay, a variable $\Delta_m = \sqrt{(M_{\Lambda\gamma_1} - M_{\Sigma^0})^2 + (M_{\bar{\Lambda}\gamma_2} - M_{\bar{\Sigma}^0})^2}$ is defined. All possible photon pairs are combined with the selected $\Lambda$ and $\bar{\Lambda}$ candidates, and the $\gamma_1$ and $\gamma_2$ candidates, which yield the smallest $\Delta_m$, are taken as the photons from the $\Sigma^0$ and $\bar{\Sigma}^0$ decays, respectively.

To suppress backgrounds, the $\Lambda\bar{\Lambda}$ invariant mass, $M_{\Lambda\bar{\Lambda}}$, is required to be within [3.05, 3.15], [2.82, 3.02], [3.63, 3.75] and [3.34, 3.61] GeV/c$^2$ for the $J/\psi \to \Lambda\bar{\Lambda}$, $J/\psi \to \Sigma^0\bar{\Sigma}^0$, $\psi(3686) \to \Lambda\bar{\Lambda}$ and $\psi(3686) \to \Sigma^0\bar{\Sigma}^0$ decays, respectively. Here the mass window requirements for the individual decay modes are determined by MC studies. In the decays $\psi \to \Lambda\bar{\Lambda}$, the $\bar{\Lambda}$ candidate is required to have mass satisfying $|M_{\bar{p}\pi^+} - M_{\bar{\Lambda}}| < 3\sigma_{M_{\bar{\Lambda}}}$, where $M_{\bar{\Lambda}}$ is the $\bar{\Lambda}$ nominal mass, and $\sigma_{M_{\bar{\Lambda}}}$ is the corresponding mass resolution, which is 2.3 MeV/$c^2$ (4.0 MeV/$c^2$) for the $J/\psi$ [$\psi(3686)$] decay. In the decays $\psi \to \Sigma^0\bar{\Sigma}^0$, the $\bar{\Sigma}^0$ candidate is required to have mass satisfying $|M_{\bar{p}\pi^+\gamma} - M_{\bar{\Sigma}^0}| < 3\sigma_{M_{\bar{\Sigma}^0}}$, where $M_{\bar{\Sigma}^0}$ is the $\bar{\Sigma}^0$ nominal mass, $\sigma_{M_{\bar{\Sigma}^0}}$ is the corresponding mass resolution, which is 4.3 MeV/$c^2$ (6.0 MeV/$c^2$) for the $J/\psi$ [$\psi(3686)$]. The candidates are further required to satisfy $\theta_{\Sigma^0\bar{\Sigma}^0} > 178°$ and $\theta_{\Sigma^0\bar{\Sigma}^0} > 178.5°$ for the $J/\psi$ and $\psi(3686)$ decays, respectively, where $\theta_{\Sigma^0\bar{\Sigma}^0}$ is the opening angle between the reconstructed $\Sigma^0$ and $\bar{\Sigma}^0$ candidates in the c.m. system.

## IV. BACKGROUND ESTIMATION

To study the backgrounds, the same selection criteria are applied to the generic inclusive $\psi$ MC samples. For the decay $J/\psi \to \Lambda\bar{\Lambda}$, the dominant backgrounds are found to be $J/\psi \to \Lambda\bar{\Sigma}^0 + \text{c.c.}$, $J/\psi \to \gamma K_s K_s$ and $J/\psi \to \gamma\eta_c$ with the subsequent decay $\eta_c \to \Lambda\bar{\Lambda}$. For the decay $J/\psi \to \Sigma^0\bar{\Sigma}^0$, the main backgrounds are from $J/\psi \to \Lambda\bar{\Sigma}^0 + \text{c.c.}$, $J/\psi \to \gamma\eta_c$ with the subsequent decay $\eta_c \to \Lambda\bar{\Lambda}, \Sigma^0\bar{\Sigma}^0, \Lambda\bar{\Sigma}^0 + \text{c.c.}$ and $J/\psi \to \Sigma^0\bar{\Sigma}^{*0} + \text{c.c.}$. For $\psi(3686) \to \Lambda\bar{\Lambda}$, the potential backgrounds are $\psi(3686) \to \pi^+\pi^- J/\psi, J/\psi \to p\bar{p}$, $\psi(3686) \to \Sigma^0\bar{\Sigma}^0$, and $\psi(3686) \to \Lambda\bar{\Sigma}^0 + \text{c.c.}$. For $\psi(3686) \to \Sigma^0\bar{\Sigma}^0$, the dominant backgrounds are from $\psi(3686) \to \gamma\chi_{cJ}, \chi_{cJ} \to \Lambda\bar{\Lambda}(J = 0, 1, 2)$ and $\psi(3686) \to \Xi^0\bar{\Xi}^0$, $\Xi^0 \to \Lambda\pi^0$, $\bar{\Xi}^0 \to \bar{\Lambda}\pi^0$. All above backgrounds can be classified into two categories, i.e. backgrounds with or without $\Lambda\bar{\Lambda}$ in the final state. The former category backgrounds are expected to produce a peak around the $\Lambda/\Sigma^0$ signal region in the $p\pi^-/p\pi^-\gamma$ invariant mass distributions and can be estimated, with the exclusive MC simulation samples using the decay branching fractions set according to the PDG [15]. The additional undetermined decays of $\eta_c \to \Sigma^0\bar{\Sigma}^0, \Lambda\bar{\Sigma}^0 + \text{c.c.}$ and $\psi(3686) \to \Lambda\bar{\Sigma}^0 + \text{c.c.}$ are estimated using the results from previous experiments for charmonium decaying to $B\bar{B}$ states (reference decays) [10,11,31], to be 1 and 0.1 times that for the decay $\eta_c \to \Lambda\bar{\Lambda}$ and 0.1 times that for $\psi(3686) \to \Lambda\bar{\Lambda}$, respectively. The contributions of other decays to the peaking background are negligible. The latter category of backgrounds are expected to be distributed smoothly in the corresponding mass distributions.

The backgrounds from continuum QED processes, i.e. $e^+e^- \to B\bar{B}$ decays, are estimated with the data samples taken at the c.m. energies of 3.08 and 3.65 GeV, which have integrated luminosities of 30 and 44 pb$^{-1}$ [18,19], respectively. By applying the same selection criteria, no event survives in the selection of $J/\psi \to B\bar{B}$, while in the selection of $\psi(3686) \to B\bar{B}$, only a few events survive, and no obvious peak is observed in the $\Lambda/\Sigma^0$ mass region. The contamination from the QCD continuum processes can be treated as nonpeaking background when determining the signal yields.

## V. RESULTS

### A. Branching fractions

With the above selection criteria, the distributions of $M_{p\pi^-}/M_{p\pi^-\gamma}$ in a range of $\pm 8$ times the mass resolution around the $\Lambda/\Sigma^0$ nominal mass in the $J/\psi$ and $\psi(3686)$

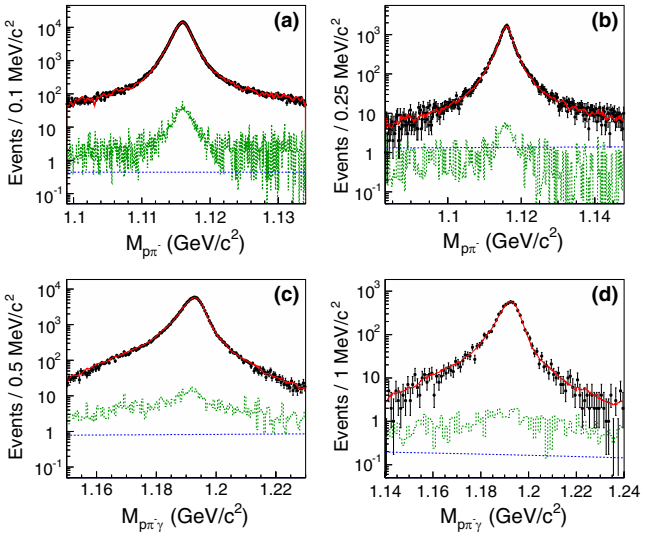


FIG. 1. The $M_{p\pi^-}$ distributions for the decays (a) $J/\psi \to \Lambda\bar{\Lambda}$ and (b) $\psi(3686) \to \Lambda\bar{\Lambda}$, and the $M_{p\pi^-\gamma}$ distributions for the decays (c) $J/\psi \to \Sigma^0\bar{\Sigma}^0$ and (d) $\psi(3686) \to \Sigma^0\bar{\Sigma}^0$, where the dots with error bars are data, the red solid curves are the overall fit results, the green dashed histograms are the backgrounds estimated with the exclusive MC simulated samples and the blue dotted line describes the remaining backgrounds.

decays are shown in Fig. 1. Clear $\Lambda/\Sigma^0$ peaks are observed with low background. To determine the signal yields, unbinned maximum likelihood fits are applied to $M_{p\pi^-}/M_{p\pi^-\gamma}$ with the mass of $\bar{p}\pi^+/\bar{p}\pi^+\gamma'$ restricted to $\pm 3$ times of resolution of $\bar{\Lambda}/\bar{\Sigma}^0$ nominal mass. In the fit, the $\Lambda/\Sigma^0$ signal shape is described by the simulated MC shape convolved with a Gaussian function to account for the difference in mass resolution between data and MC simulation. The peaking backgrounds are described with the shapes from exclusive MC simulations with fixed magnitudes according to the branching fractions of background listed in the PDG [15], and the nonpeaking backgrounds are described with second-order polynomial functions with free parameters in the fit. The fit results are illustrated in Fig. 1, and the corresponding signal yields are summarized in Table III.

The branching fractions are calculated using

$$\mathcal{B}(\psi \to B\bar{B}) = \frac{N_{\rm obs}}{N_\psi \cdot \epsilon \cdot \mathcal{B}_i}, \qquad (3)$$

where $N_{\rm obs}$ is the number of signal events minus peaking background, $\epsilon$ is the detection efficiency, which is estimated with MC simulation incorporating the $\cos\theta$ distributions obtained in this analysis and the scale factors to account for the difference in efficiency between data and MC simulation as described below, $\mathcal{B}_i$ is the product of branching fractions for the intermediate states in the cascade decay from the PDG [15] and $N_\psi$ is the total number of $\psi$ events estimated by counting the inclusive hadronic events [18,19]. The corresponding detection efficiencies and the resultant branching fractions are also summarized in Table III.

### B. Angular distributions

The baryon $\cos\theta$ distributions in the c.m. system corrected by detection efficiency are shown in Fig. 2, and the signal yields in each of the 20 bins are determined with the same method as that in the branching fraction measurements. The detection efficiencies in each bin are estimated with the signal MC samples and scaled with correction factors to compensate for the efficiency difference between data and MC simulation. The efficiency corrected $\cos\theta$ distributions are fitted with Eq. (2) with a least-squares method, the corresponding fit results are shown in Fig. 2 and the resultant $\alpha$ values are summarized in Table III.

The correction factors used to correct for the efficiency differences between data and MC simulation as a function of $\cos\theta$ are determined by studying various control samples, where $\theta$ is the polar angle of the hyperon. The efficiency differences are due to differences in the efficiencies of charged particle tracking, photon detection and hyperon reconstruction. For example, the efficiencies related with charged particle tracking and $\Lambda$ reconstruction are studied with a special control sample of $\psi \to \Lambda\bar{\Lambda}$ events, where a $\bar{\Lambda}$ tag has been reconstructed. Events with two or more charged tracks, in which a $\bar{p}$ and $\pi^+$ have been identified using particle identification, are selected. The $\bar{\Lambda}$ tag candidate must satisfy a secondary vertex fit, have a decay length greater than 0.2 cm and satisfy mass and momentum requirements. The numbers of tagged $\Lambda$ events, $N_{\rm tag}$, are obtained by fitting the $\Lambda$ peak in the distribution of invariant mass recoiling against the $\bar{\Lambda}$ tag. The numbers of $\Lambda$ signal events, $N_{\rm sig}$, are obtained by fitting the recoil mass

TABLE III. The numbers of observed signal events $N_{\rm obs}$, the corrected detection efficiency $\epsilon$, the numbers of peaking backgrounds $N_{\rm pk}$, the numbers of smooth backgrounds $N_{\rm sm}$, the resultant $\alpha$ values for the angular distributions and the branching fractions $\mathcal{B}$, where the errors are statistical only.

| Channel | $N_{\rm obs}$ | $\epsilon$ (%) | $N_{\rm pk}$ | $N_{\rm sm}$ | $\alpha$ | $\mathcal{B}$ ($\times 10^{-4}$) |
|---|---|---|---|---|---|---|
| $J/\psi \to \Lambda\bar{\Lambda}$ | $440,675 \pm 670$ | $42.37 \pm 0.14$ | 1,819 | $154 \pm 166$ | $0.469 \pm 0.026$ | $19.43 \pm 0.03$ |
| $J/\psi \to \Sigma^0\bar{\Sigma}^0$ | $111,026 \pm 335$ | $17.83 \pm 0.06$ | 820 | $131 \pm 12$ | $-0.449 \pm 0.020$ | $11.64 \pm 0.04$ |
| $\psi(3686) \to \Lambda\bar{\Lambda}$ | $31,119 \pm 187$ | $42.83 \pm 0.34$ | 252 | $352 \pm 65$ | $0.824 \pm 0.074$ | $3.97 \pm 0.02$ |
| $\psi(3686) \to \Sigma^0\bar{\Sigma}^0$ | $6,612 \pm 82$ | $14.79 \pm 0.12$ | 89 | $17 \pm 5$ | $0.71 \pm 0.11$ | $2.44 \pm 0.03$ |

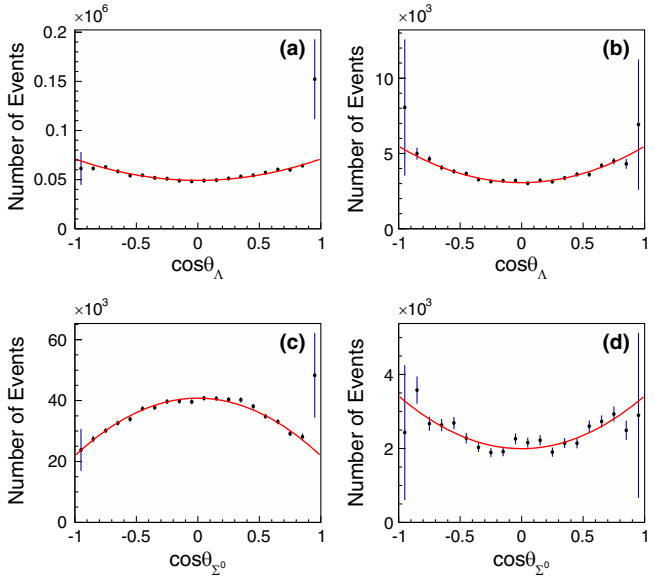


FIG. 2. The distributions of efficiency corrected polar angle of the baryon for the decays (a) $J/\psi \to \Lambda\bar{\Lambda}$, (b) $\psi(3686) \to \Lambda\bar{\Lambda}$, (c) $J/\psi \to \Sigma^0\bar{\Sigma}^0$ and (d) $\psi(3686) \to \Sigma^0\bar{\Sigma}^0$, where the dots with error bars are data and the red solid curves are the fit results.

distribution for events where, in addition, a $\Lambda$ signal is reconstructed on the recoil side, which requires two oppositely charged tracks that satisfy a vertex fit and have a decay length greater than 0.2 cm. The combined efficiency of charged tracking (proton and pion) and $\Lambda$ reconstruction is then $N_{\rm sig}/N_{\rm tag}$. The ratios of the data and MC simulation efficiencies as a function of $\cos\theta$ are taken as the correction factors. The $\bar{\Lambda}$ correction factors are determined in an analogous way using $\psi \to \Lambda\bar{\Lambda}$ events with a $\Lambda$ tag. The overall correction factor in the different $\cos\theta$ bins is the product of the $\Lambda$ and $\bar{\Lambda}$ correction factors.

In an analogous way, the combined efficiency of photon detection and $\Sigma^0$ reconstruction is studied with a control sample of $\psi \to \Sigma^0\bar{\Sigma}^0$ events, which have a $\bar{\Sigma}^0$ tag and an additional $\Lambda$. Events are selected that have a $\Lambda$ and $\bar{\Lambda}$ using the same criteria as above and at least one additional photon. The $\bar{\Lambda}$ and photon must have an invariant mass consistent with that of a $\bar{\Sigma}^0$. The numbers of tagged $\Sigma^0$ events are obtained by fitting the $\Sigma^0$ peak in the distribution of mass recoiling against the $\bar{\Sigma}^0$ tag. We then search for another photon and reconstruct the $\Sigma^0$ by requiring the invariant mass of the photon and tagged $\Lambda$ be consistent with the $\Sigma^0$ mass. The number of events with a $\Sigma^0$ signal divided by the number of tagged $\Sigma^0$ events is the combined efficiency of photon detection and $\Sigma^0$ reconstruction. The ratios of detection efficiencies in the different $\cos\theta$ bins between data and MC simulation determine the correction factors. The overall correction factor in the different $\cos\theta$ bins is the product of the $\Sigma^0$, $\bar{\Sigma}^0$, $\Lambda$ and $\bar{\Lambda}$ correction factors.

## VI. SYSTEMATIC UNCERTAINTY

### A. Branching fraction

Systematic uncertainties in the branching fraction measurements are mainly due to the differences of detection efficiency and resolution between data and MC simulation. The sources of uncertainty related with the detection efficiency include charged tracking, photon detection and $\Lambda/\Sigma^0$ reconstruction. The sources of uncertainty due to the resolution difference include the $M_{\Lambda\bar{\Lambda}}$ and $M_{\bar{\Lambda}}/M_{\bar{\Sigma}^0}$ mass requirements, and the opening angle $\theta_{\Sigma^0\bar{\Sigma}^0}$ requirement in the decays $\psi \to \Sigma^0\bar{\Sigma}^0$. Additional uncertainty sources including the model of the baryon polar angular distribution, the fit procedure, the decay branching fractions of $\Lambda/\Sigma^0$ states and the total number of $\psi$ events are also considered. All of the systematic uncertainties are studied in detail as discussed in the following:

(1) As described above, the detection efficiencies related with the tracking, photon detection and $\Lambda/\Sigma^0$ reconstruction are corrected bin by bin in $\cos\theta$ to decrease the difference between data and MC simulation. The overall correction factors, which are determined with control samples, are $0.9974 \pm 0.0041$, $0.9936 \pm 0.0064$, $0.980 \pm 0.011$ and $0.954 \pm 0.022$ for the decays $J/\psi \to \Lambda\bar{\Lambda}$, $J/\psi \to \Sigma^0\bar{\Sigma}^0$, $\psi(3686) \to \Lambda\bar{\Lambda}$ and $\psi(3686) \to \Sigma^0\bar{\Sigma}^0$, respectively. To estimate the corresponding uncertainties, the correction factors are changed by $\pm 1$ standard deviations, and the resultant changes in the branching fractions are taken as the systematic uncertainties.

(2) The uncertainties related with the $M_{\Lambda\bar{\Lambda}}$ requirement are estimated by varying the mass requirement edges by $\pm 10$ MeV/$c^2$. The uncertainties related with the $\bar{\Lambda}/\bar{\Sigma}^0$ mass requirement are estimated by changing the requirement by $\pm 1$ times the mass resolution. The uncertainties due to the requirement on the opening angle $\theta_{\Sigma^0\bar{\Sigma}^0}$ in the decays $\psi \to \Sigma^0\bar{\Sigma}^0$ are estimated by changing the requirement to be 175°. The relative changes in the branching fractions are individually taken as the systematic uncertainties.

(3) MC simulations indicate that the detection efficiencies depend on the distributions of baryon polar angular $\cos\theta$. In the analysis, the measured $\alpha$ values are used for the $\cos\theta$ distributions in the MC simulation. Alternative MC samples are generated by changing the $\alpha$ values by $\pm 1$ standard deviations and are used to estimate the detection efficiencies. The resultant changes in the detection efficiencies with respect to their nominal values are taken as the systematic uncertainties.

(4) The sources of systematic uncertainty associated with the fit procedure include the fit range, the signal shape and the modeling of backgrounds. The uncertainties related with the fit range are estimated by

changing the range by $\pm 1$ times the mass resolution for the fits. The signal shapes are modeled with the signal MC simulated shapes convolved with a Gaussian function in the nominal fit. The corresponding uncertainties are estimated with alternative fits with different signal shapes, i.e. a Breit-Wigner function convolved with a Gaussian function for $\Lambda$ and with a crystal ball function [32] for $\Sigma^0$, where the Gaussian function and crystal ball function represent the corresponding mass resolutions. The uncertainties related with the peaking backgrounds, which are estimated with the exclusive MC samples in the nominal fits, are studied by changing the branching fractions of the individual background, or by changing the branching fractions for the reference decays which the estimated branching fractions for the undetermined backgrounds are based on, by $\pm 1$ times their uncertainties from the PDG [15]. The uncertainties associated with the nonpeaking backgrounds are estimated with alternative fits by replacing the second-order polynomial function with a first-order polynomial function. The resultant changes from the above changes in the signal yields are taken individually as the systematic uncertainties.

(5) The uncertainties related with the branching fractions of baryon and antibaryon decays are taken from the PDG [15]. The total numbers of $\psi$ events are obtained by studying the inclusive hadronic events, and their uncertainties are 0.6% and 0.7% for the $J/\psi$ and $\psi(3686)$ data samples [18–20], respectively.

The various systematic uncertainties in the branching fraction measurements are summarized in Table IV. The total systematic uncertainties are obtained by summing the individual values in quadrature.

TABLE IV. Systematic uncertainties in the measurement of branching fractions.

| | $J/\psi$ | | $\psi(3686)$ | |
|---|---|---|---|---|
| | $\Lambda\bar{\Lambda}$ (%) | $\Sigma^0\bar{\Sigma}^0$ (%) | $\Lambda\bar{\Lambda}$ (%) | $\Sigma^0\bar{\Sigma}^0$ (%) |
| Efficiency correction | 0.5 | 0.7 | 1.2 | 2.3 |
| $M_{\Lambda\bar{\Lambda}}$ requirement | 0.1 | 0.1 | 0.1 | 0.2 |
| $\bar{\Lambda}/\bar{\Sigma}^0$ mass requirement | 0.1 | 0.3 | 0.3 | 0.2 |
| $\theta_{\Sigma^0\bar{\Sigma}^0}$ requirement | ... | 0.3 | ... | 0.2 |
| Baryon polar angle | 0.8 | 0.9 | 2.0 | 3.1 |
| Fit range | 0.1 | 0.1 | 0.2 | 0.2 |
| Signal shape | 0.1 | 0.3 | 0.1 | 0.2 |
| Peaking background | 0.3 | 0.4 | 0.3 | 1.2 |
| Nonpeaking background | 0.1 | 0.1 | 0.3 | 0.2 |
| Branching fractions | 1.2 | 1.2 | 1.2 | 1.2 |
| $N_{J/\psi}/N_{\psi(3686)}$ | 0.6 | 0.6 | 0.7 | 0.7 |
| Total | 1.7 | 1.9 | 2.8 | 4.3 |

### B. Angular distribution

The sources of systematic uncertainties in the baryon polar angular measurements include the signal yields in different $\cos\theta$ intervals and the $\cos\theta$ fit procedure. The MC statistics and correction errors are already included in the error referred to as "statistical."

(1) In the polar angular measurements, the signal yield in a given $\cos\theta$ interval is obtained with the same fit method as that used in the branching fraction measurements. The uncertainties of the signal yield in each $\cos\theta$ bin are mainly from the fit range, the signal shape and the background modeling. We individually estimate the uncertainty of the signal yield in each $\cos\theta$ interval with the same methods as those used in the branching fraction measurements for the different uncertainty sources, and then repeat the $\cos\theta$ fit procedure with the changed signal yields. The resultant changes in the $\alpha$ values with respect to the nominal values are taken as systematic uncertainties.

(2) The sources of systematic uncertainty related to the $\cos\theta$ fit procedure include the fit range and the number of bins in the $\cos\theta$ distribution. We repeat the fit procedures with the alternative fit range $[-0.9, 0.9]$ and alternative number of bins (40). The resultant changes of $\alpha$ values are taken as the systematic uncertainties.

The individual absolute uncertainties in the polar angular distribution measurements are summarized in Table V. The total systematic uncertainties are obtained by summing the individual values in quadrature.

## VII. SUMMARY

In summary, using the data samples of $1310.6 \times 10^6$ $J/\psi$ events and $447.9 \times 10^6$ $\psi(3686)$ events collected with the BESIII detector at the BEPCII collider, the $J/\psi$ and $\psi(3686)$ decaying into $\Lambda\bar{\Lambda}$ and $\Sigma^0\bar{\Sigma}^0$ pairs are studied. The decay branching fractions and $\alpha$ values are measured, and the results are summarized in Table VI. The branching fractions for $J/\psi$ decays are in good agreement with the

TABLE V. Absolute systematic uncertainties in the measurement of $\alpha$.

| | $J/\psi$ | | $\psi(3686)$ | |
|---|---|---|---|---|
| | $\Lambda\bar{\Lambda}$ | $\Sigma^0\bar{\Sigma}^0$ | $\Lambda\bar{\Lambda}$ | $\Sigma^0\bar{\Sigma}^0$ |
| Mass fit range | 0.001 | 0.001 | 0.003 | 0.005 |
| Signal shape | 0.001 | 0.002 | 0.001 | 0.003 |
| Peaking background | 0.006 | 0.005 | 0.006 | 0.015 |
| Nonpeaking background | 0.002 | 0.001 | 0.004 | 0.002 |
| $\alpha$ fit range | 0.001 | 0.003 | 0.007 | 0.019 |
| Number of bins | 0.004 | 0.005 | 0.001 | 0.024 |
| Total | 0.008 | 0.008 | 0.011 | 0.035 |

TABLE VI. Results for measured $\alpha$ values and branching fractions $\mathcal{B}$ in this analysis. The first uncertainties are statistical and the second are systematic.

| Channel | $\alpha$ | $\mathcal{B}$ ($\times 10^{-4}$) |
|---|---|---|
| $J/\psi \to \Lambda\bar{\Lambda}$ | $0.469 \pm 0.026 \pm 0.008$ | $19.43 \pm 0.03 \pm 0.33$ |
| $J/\psi \to \Sigma^0\bar{\Sigma}^0$ | $-0.449 \pm 0.020 \pm 0.008$ | $11.64 \pm 0.04 \pm 0.23$ |
| $\psi(3686) \to \Lambda\bar{\Lambda}$ | $0.82 \pm 0.08 \pm 0.02$ | $3.97 \pm 0.02 \pm 0.12$ |
| $\psi(3686) \to \Sigma^0\bar{\Sigma}^0$ | $0.71 \pm 0.11 \pm 0.04$ | $2.44 \pm 0.03 \pm 0.11$ |

results of BESII [10] and *BABAR* [12] experiments, and those for $\psi(3686)$ decays are in agreement with the results of CLEO [9], BESII [11] and Dobbs *et al.* [13] with a maximum of 2 times the standard deviations. The earlier experimental results [5–8] have significant differences with those of this analysis. The precisions of our branching fraction results are much improved than those of previous experiments listed in Table I. The $\alpha$ values in the decays $\psi(3686) \to \Lambda\bar{\Lambda}$ and $\psi(3686) \to \Sigma^0\bar{\Sigma}^0$ are measured for the first time, while those of $J/\psi \to \Lambda\bar{\Lambda}$ and $J/\psi \to \Sigma^0\bar{\Sigma}^0$ decays are of much improved precision compared to previous measurements. It is worth noting that the $\alpha$ value in the decay $J/\psi \to \Sigma^0\bar{\Sigma}^0$ is negative, which confirms the results in Ref. [10].

To test the 12% rule, we also obtain the Q values to be $\frac{\mathcal{B}(\psi(3686)\to\Lambda\bar{\Lambda})}{\mathcal{B}(J/\psi\to\Lambda\bar{\Lambda})} = (20.43 \pm 0.11 \pm 0.58)\%$ and $\frac{\mathcal{B}(\psi(3686)\to\Sigma^0\bar{\Sigma}^0)}{\mathcal{B}(J/\psi\to\Sigma^0\bar{\Sigma}^0)} = (20.96 \pm 0.27 \pm 0.92)\%$, where the common systematic uncertainties between $J/\psi$ and $\psi(3686)$ decays are canceled. The Q values are of high precision, and differ from the expectation from pQCD by more than 3 standard deviations.

## ACKNOWLEDGMENTS

The BESIII Collaboration thanks the staff of BEPCII and the IHEP computing center for their strong support. This work is supported in part by the National Key Basic Research Program of China under Contracts No. 2009CB825200 and No. 2015CB856700; the National Natural Science Foundation of China (NSFC) under Contracts No. 10905034, No. 10935007, No. 11125525, No. 11235011, No. 11322544, No. 11335008 and No. 11425524; the Chinese Academy of Sciences (CAS) Large-Scale Scientific Facility Program; the CAS Center for Excellence in Particle Physics (CCEPP); the Collaborative Innovation Center for Particles and Interactions (CICPI); Joint Large-Scale Scientific Facility Funds of the NSFC and CAS under Contracts No. 11179007, No. U1232106, No. U1232201, No. U1332201; the Natural Science Foundation of Shandong Province under Contract No. ZR2009AQ002; the CAS under Contracts No. KJCX2-YW-N29 and No. KJCX2-YW-N45; the 100 Talents Program of CAS; the National 1000 Talents Program of China; INPAC and Shanghai Key Laboratory for Particle Physics and Cosmology; German Research Foundation DFG under Contract No. Collaborative Research Center CRC-1044, FOR-2359; Istituto Nazionale di Fisica Nucleare, Italy; Joint Funds of the National Science Foundation of China under Contract No. U1232107; the Ministry of Development of Turkey under Contract No. DPT2006K-120470; the Russian Foundation for Basic Research under Contract No. 14-07-91152; the Swedish Research Council; the U.S. Department of Energy under Contracts No. DE-FG02-04ER41291, No. DE-FG02-05ER41374, No. DE-SC0012069 and No. DESC0010118; the U.S. National Science Foundation; University of Groningen (RuG) and the Helmholtzzentrum fuer Schwerionenforschung GmbH (GSI), Darmstadt; and the WCU Program of National Research Foundation of Korea under Contract No. R32-2008-000-10155-0.

[1] P. Kessler, Nucl. Phys. **B15**, 253 (1970); S. J. Brodsky and G. P. Lepage, Phys. Rev. D **24**, 2848 (1981).
[2] T. Appelquist and H. D. Politzer, Phys. Rev. Lett. **34**, 43 (1975); A. De Rujula and S. L. Glashow, Phys. Rev. Lett. **34**, 46 (1975); W. S. Hou, Phys. Rev. D **55**, 6952 (1997).
[3] M. E. B. Franklin *et al.* (MARKII Collaboration), Phys. Rev. Lett. **51**, 963 (1983).
[4] Y. F. Gu and X. H. Li, Phys. Rev. D **63**, 114019 (2001); X. H. Mo, C. Z. Yuan, and P. Wang, High Energy Phys. Nucl. Phys. **31**, 686 (2007); N. Brambilla *et al.* (Quarkonium Working Group), Eur. Phys. J. C **71**, 1534 (2011); Q. Wang, G. Li, and Q. Zhao, Phys. Rev. D **85**, 074015 (2012).
[5] M. W. Eaton *et al.* (MARKII Collaboration), Phys. Rev. D **29**, 804 (1984).
[6] D. Pallin *et al.* (DM2 Collaboration), Nucl. Phys. **B292**, 653 (1987).
[7] J. Z. Bai *et al.* (BES Collaboration), Phys. Lett. B **424**, 213 (1998).
[8] J. Z. Bai *et al.* (BES Collaboration), Phys. Rev. D **63**, 032002 (2001).
[9] T. K. Pedlar *et al.* (CLEO Collaboration), Phys. Rev. D **72**, 051108 (2005).
[10] M. Ablikim *et al.* (BESII Collaboration), Phys. Lett. B **632**, 181 (2006).
[11] M. Ablikim *et al.* (BESII Collaboration), Phys. Lett. B **648**, 149 (2007).
[12] B. Aubert *et al.* (*BABAR* Collaboration), Phys. Rev. D **76**, 092006 (2007).

[13] S. Dobbs, A. Tomaradze, T. Xiao, K. K. Seth, and G. Bonvicini, Phys. Lett. B **739**, 90 (2014).
[14] M. Ablikim *et al.* (BESIII Collaboration), Phys. Rev. D **93**, 072003 (2016); arXiv:1612.08664.
[15] K. A. Olive *et al.* (Particle Data Group), Chin. Phys. C **38**, 090001 (2014).
[16] M. Claudson, S. L. Glashow, and M. B. Wise, Phys. Rev. D **25**, 1345 (1982).
[17] C. Carimalo, Int. J. Mod. Phys. A **02**, 249 (1987).
[18] M. Ablikim *et al.* (BESIII Collaboration), Chin. Phys. C **36**, 915 (2012); **41**, 013001 (2017).
[19] M. Ablikim *et al.* (BESIII Collaboration), Chin. Phys. C **37**, 063001 (2013).
[20] The total number of $\psi(3686)$ events taken at 2009 and 2012 is obtained based on the same method. The preliminary number is determined to be $447.9 \times 10^6$ with uncertainties of 0.7%.
[21] M. Ablikim *et al.* (BESIII Collaboration), Nucl. Instrum. Methods Phys. Res., Sect. A **614**, 345 (2010).
[22] C. Zhang, Sci. China, Ser. G: Phys., Mech. Astron. **53**, 2084 (2010).
[23] D. M. Asner *et al.*, Int. J. Mod. Phys. A **24**, 499 (2009).
[24] S. Agostinelli *et al.* (GEANT4 Collaboration), Nucl. Instrum. Methods Phys. Res., Sect. A **506**, 250 (2003).
[25] Z. Y. Deng *et al.*, High Energy Phys. Nucl. Phys. **30**, 371 (2006).
[26] W. D. Li, Y. J. Mao, and Y. F. Wang, Int. J. Mod. Phys. A **24**, 9 (2009).
[27] S. Jadach, B. F. L. Ward, and Z. Was, Comput. Phys. Commun. **130**, 260 (2000); Phys. Rev. D **63**, 113009 (2001).
[28] D. J. Lange, Nucl. Instrum. Methods Phys. Res., Sect. A **462**, 152 (2001); R. G. Ping, Chin. Phys. C **32**, 243 (2008).
[29] J. C. Chen, G. S. Huang, X. R. Qi, D. H. Zhang, and Y. S. Zhu, Phys. Rev. D **62**, 034003 (2000).
[30] M. Xu *et al.*, Chin. Phys. C **33**, 1381 (2009).
[31] M. Ablikim *et al.* (BESIII Collaboration), Phys. Rev. D **86**, 032014 (2012).
[32] J. Cheng, Z. Wang, L. Lebanowski, G. Lin, and S. Chen, Nucl. Instrum. Methods Phys. Res., Sect. A **827**, 165 (2016).